Available online at www.sciencedirect.com
ScienceDirect
International Journal of Heat and Mass Transfer 51 (2008) 3535–3547
International Journal of HEAT and MASS TRANSFER
www.elsevier.com/locate/ijhmt

Thermo-bioconvection in a suspension of gravitactic micro-organisms in vertical cylinders

M. Taheri, E. Bilgen *

Ecole Polytechnique, University of Montreal, C.P. 6079, Centre-ville, Montréal, QC, Canada H3C 3A7

Received 21 May 2007; received in revised form 19 October 2007
Available online 31 December 2007

Abstract

We investigate the effect of heating or cooling from below at constant temperature and constant heat flux on the development of gravitactic bioconvection in vertical cylinders with stress free sidewalls. The governing equations are the continuity equation, the Navier–Stokes equations with the Boussinesq approximation, the diffusion equation for the motile micro-organisms and the energy equation. The control volume method is used to solve numerically the complete set of governing equations. The governing parameters are the thermal and bioconvection Rayleigh numbers, the bioconvection Peclet number, the Lewis number, the Schmidt number and the aspect ratio. We found that subcritical bifurcations of bioconvection became supercritical bifurcations when the thermal Rayleigh number Ra_T is different than zero. For $Ra_T < 0$, i.e. for cooling from below, we have opposing buoyancy forces, the convection is decreased and the critical thermo-bioconvection Rayleigh number is increased with respect to that of bioconvection. For $Ra_T > 0$, i.e. for heating from below, we have cooperating buoyancy forces, the convection is increased and the critical thermo-bioconvection Rayleigh number is decreased with respect to that of bioconvection. Heating and cooling from below at constant temperature and heat flux modify considerably the pattern formation of the gravitactic bioconvection.
© 2007 Elsevier Ltd. All rights reserved.

Keywords: Thermo-bioconvection; Gravitactic micro-organisms; Heated layer; Vertical cylinders

1. Introduction

Bioconvection is the spontaneous pattern formation in suspensions of micro-organisms which are little denser than water and move randomly, but on the average, upward against gravity. Up swimming of micro-organisms is generally a response to an external force field such as gravity (gravitaxis or geotaxis), torques due to shear and gravity (gyrotaxis), biochemical stimulus such as gradient of oxygen concentration (chemotaxis) and light source (phototaxis) (e.g. [1–4]). Due to up swimming, the top layer of the suspension becomes denser than the layer below, resulting in an unstable density distribution. This may lead to a convective instability or overturning type of instability and formation of convection patterns similar to the patterns observed in Rayleigh–Bénard convection. Theoretical models of bioconvection for different types of motile micro-organisms have been developed in various publications. Pedley and Kessler [5], Hill and Pedley [6] have presented reviews on this subject.

Rational continuum models for a suspension of purely gravitactic micro-organisms have been formulated and analyzed by Childress et al. [1]. A numerical study based on the continuum models was presented by Fujita and Watanabe [7]. Numerical experiments were carried out on the gravitactic bioconvection in a rectangular cavity by Harashima et al. [8]. They showed that the system evolves in the direction of intensifying downward advection of micro-organisms and reducing the total potential energy of the system. Ghorai and Hill [9–12] studied gyrotactic bioconvection in a series of papers using a vorticity–stream function formulation of the basic model first introduced by

* Corresponding author. Tel.: +1 514 340 4711x4579; fax: +1 514 340 5917.
E-mail address: bilgen@polymtl.ca (E. Bilgen).

0017-9310/$ - see front matter © 2007 Elsevier Ltd. All rights reserved.
doi:10.1016/j.ijheatmasstransfer.2007.10.023

Nomenclature

A	cavity aspect ratio, $A = R/H$
D_c	cell diffusivity
$\vec{g}$	gravitational acceleration
H	cavity height
$\vec{J}$	dimensionless flux of micro-organisms
$\vec{k}$	unit vertical vector
R	cylinder radius
Le	Lewis number, $Le = \alpha/D_c$
n	dimensionless cell concentration
$\bar{n}$	average cell concentration
$\vec{n}$	unit normal vector to the boundaries
p	dimensionless pressure
Pe	bioconvection Peclet number, $Pe = HV_c/D_c$
q	dimensionless heat flux, $q = \frac{\partial T}{\partial z}$
Ra	bioconvection Rayleigh number, $Ra = g\vartheta\Delta\rho\bar{n}H^3/\rho\nu D_c$
Ra_c	critical bioconvection Rayleigh number
Ra_T	thermal Rayleigh number, $Ra_T = g\beta\Delta TH^3/\nu\alpha$ or $Ra_T = g\beta qH^4/\nu\alpha k$
Ra_{Tc}	critical thermal Rayleigh number for heating or cooling from below
Sc	Schmidt number, $Sc = \nu/D_c$
T	dimensionless temperature
t	dimensional variable
$\vec{u}$	dimensionless fluid velocity
V_c	gravitactic cell velocity
(r, z)	dimensionless coordinate system

Greek symbols

α	thermal diffusivity
β	volume expansion coefficient
ω	dimensionless vorticity
μ	dynamic viscosity of the suspension
ν	kinematic viscosity of the suspension
ρ_w	water density
ρ_c	cell density
$\Delta\rho$	difference between cell and water densities, $\Delta\rho = \rho_c - \rho_w$
ϑ	cell volume
ψ	dimensionless stream function

Superscripts

$'$	dimensional variable
sub	subcritical
sup	supercritical

Subscripts

ext	extremum
max	maximum
min	minimum

Pedley et al. [13]. They examined the development and instabilities of two-dimensional gyrotactic plumes. Cases with different initial conditions and different width-to-height ratios of a deep enclosure were compared.

Recently, a number of theoretical analyses of thermo-bioconvection of a suspension of gyrotactic and oxytactic micro-organisms have been carried out by Kuznetsov [14–16]. The effect of the temperature gradient on the stability of a suspension of motile gyrotactic micro-organisms in a fluid layer was investigated [14]. It is suggested that this problem may be relevant to motile thermophilic micro-organisms that live in hot springs. The author found that a suspension of gyrotactic micro-organisms in a horizontal fluid layer heated from below is less stable than the same suspension under isothermal conditions. In a complementary study [14], Nield and Kuznetsov [17] investigated the case where the layer is cooled from below. They presented a linear stability analysis of a suspension of gyrotactic micro-organisms in fluid layer of finite depth. They found that cooling from below stabilizes the suspension and oscillatory convection is possible in certain circumstances. Alloui et al. [18] carried out a linear stability analysis of the thermo-bioconvection in suspension of gravitactic micro-organisms in shallow fluid layers. The effect of heating or cooling from below on the stability was investigated. They found that the thermal effect may stabilize or destabilize the suspension and change the wave length of the bio-convection pattern. In a subsequent study [19], they investigated numerically thermo-bioconvection in a square cavity and found that the bioconvection was stabilized when cooled from below while destabilized by heating below. They observed that there was a transition from subcritical to supercritical when the Rayleigh number was increased.

We see from this brief review that there are as yet no numerical simulations of thermo-bioconvection flows above the critical Rayleigh numbers, and on the effect of the temperature gradient on the bifurcation and stability of gravitactic bioconvection in vertical cylinders. In this paper, we will investigate the development of thermo-bioconvection in vertical cylinders with stress free sidewalls by numerical simulation. We will focus on the effect of heating or cooling from below in case of (i) isothermal and (ii) constant heat flux, and we will investigate the thermal effect on the bifurcation characteristics of the gravitactic micro-organisms and examine the thermo-bioconvection above the critical Rayleigh numbers.

2. Mathematical formulation

The system consists of a suspension of gravitactic micro-organisms enclosed in a cylindrical enclosure of radius R and height H referred to cylindrical Cartesian coordinates (r, z) with the z-axis pointing vertically upwards. The verti-

cal walls of the enclosure are stress free and the top and bottom walls are rigid. There is no flux of cells through any of the walls. The coordinate system, computational domain and the boundary conditions are shown in Fig. 1.

We assume that the fluid is incompressible and the flow is axisymmetric. The concentration distribution is uniform and each cell has a volume ϑ and density ρ_c. The two-dimensional continuity and Navier–Stokes equations with the Boussinesq approximation, cell conservation equation and energy equation are solved

$$\nabla \cdot \vec{u}' = 0 \tag{1}$$

$$\rho_w \frac{\partial \vec{u}'}{\partial t'} + \rho_w \nabla \cdot (\vec{u}'\vec{u}') = -\nabla p' + \mu \nabla^2 \vec{u}' + \vartheta \Delta\rho n' \vec{g} - \rho_w \beta (T' - T_0)\vec{g} \tag{2}$$

$$\frac{\partial n'}{\partial t'} = -\nabla \vec{J}' \quad \text{with} \quad \vec{J}' = (\vec{u}' + V_c \vec{k}) n' - D_c \nabla n' \tag{3}$$

$$\frac{\partial T'}{\partial t'} + \nabla \cdot (\vec{u}' T') = \alpha \nabla^2 T' \tag{4}$$

By using the vorticity stream function formulation, these equations are made dimensionless using the length scale H, the time scale of H^2/D_c, the velocity scale of D_c/H, the concentration scale $\bar{n}$ and the temperature scale ΔT. The resulting system of coupled non-dimensional equations is

$$\omega = -\nabla^2 \psi \tag{5}$$

$$\frac{\partial \omega}{\partial t} + \frac{\partial (u\omega)}{\partial r} + \frac{\partial (v\omega)}{\partial z} = Sc\left(\nabla^2 \omega - \frac{\omega}{r^2}\right) + Sc\left(Ra \frac{\partial n}{\partial r} - Ra_T Le \frac{\partial T}{\partial r}\right) \tag{6}$$

$$\frac{\partial n}{\partial t} + u\frac{\partial n}{\partial r} + (v + Pe)\frac{\partial n}{\partial z} = \nabla^2 n \tag{7}$$

$$\frac{\partial T}{\partial t} + u\frac{\partial T}{\partial r} + v\frac{\partial T}{\partial z} = Le \nabla^2 T \tag{8}$$

The governing parameters of the problem are the Schmidt number, $Sc = \nu/D_c$, the bioconvection Rayleigh number, $Ra = g\vartheta\Delta\rho\bar{n}PeH^3/\rho\nu D_c$, the thermal Rayleigh numbers, $Ra_T = g\beta\Delta T H^3/\nu\alpha$ and $Ra_T = g\beta q H^4/\nu\alpha\, k$, the Lewis number, $Le = \alpha/D_c$, and the bioconvection Peclet number, $Pe = HV_c/D_c$.

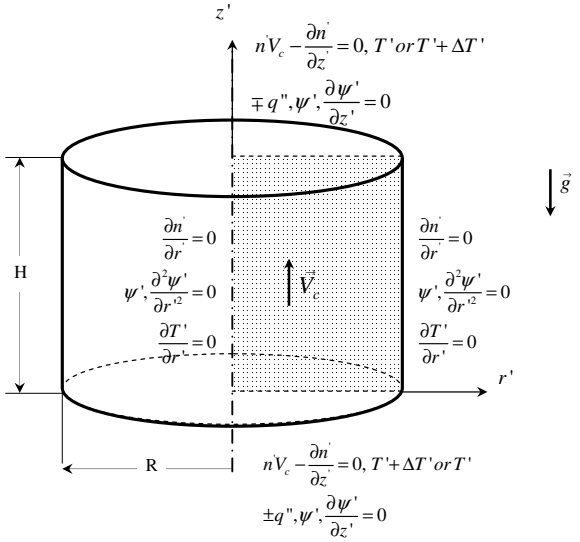

Fig. 1. Coordinate system, computational domain and boundary conditions.

With reference to Fig. 1, we impose rigid, no-slip boundary conditions at the bottom and top walls, and assume that the vertical boundaries as well as the symmetry centerline are stress free, so that

$$\psi = 0, \quad \frac{\partial \psi}{\partial z} = 0 \quad \text{at } z = 0, 1 \tag{9}$$

$$\psi = 0, \quad \frac{\partial^2 \psi}{\partial r^2} = 0 \quad \text{at } r = 0, A \tag{10}$$

At the impermeable boundaries, the condition of zero-flux $\vec{J} \cdot \vec{n} = 0$ are applied, i.e.

$$nPe - \frac{\partial n}{\partial z} = 0 \quad \text{at } z = 0, 1 \tag{11}$$

$$\frac{\partial n}{\partial r} = 0 \quad \text{at } r = 0, A \tag{12}$$

The thermal boundary conditions are isothermal or constant heat flux on horizontal boundaries and adiabatic at vertical boundaries as well as at the symmetry centerline. Hence,

$$T = 1 \text{ or } 0, \quad q = 1 \text{ or } -1 \quad \text{at } z = 0 \tag{13}$$

$$T = 0 \text{ or } 1, \quad q = 1 \text{ or } -1 \quad \text{at } z = 1 \tag{14}$$

$$\frac{\partial T}{\partial r} = 0 \quad \text{at } r = 0, A \tag{15}$$

The initial condition is

$$n = 1, \quad T = 0 \quad \text{at } t = 0 \tag{16}$$

3. Numerical procedure

The control volume method [20] is used to discretize the governing equations (5)–(8) with a uniform staggered grid. The stream function is stored on one set of nodes and the vorticity, concentration and temperature are stored on another set of nodes. The discretized equations are derived using the central differences for spatial derivatives and backward differences for time derivatives. A line-by-line tri-diagonal matrix algorithm with relaxation is used in conjunction with iteration to solve the nonlinear discretized equations. The convergence is reached when

$$\frac{|f_{i,j}^{m+1} - f_{i,j}^{m}|}{\max |f_{i,j}^{m}|} \leqslant \varepsilon \tag{17}$$

where f corresponds to the variables (ω, ψ, n, T) and ε is the prescribed tolerance, m is the iteration number, and i,j denote the grid points.

Uniform grid in x and y directions were used for all computations. Grid convergence was studied for the case of $A = 0.5$, $Ra_T = 0$, $Ra = 1000$, $Sc = 1$ and $Pe = 10$, the grid size was varied from 26×51 to 101×201. The result of this study is presented in Table 1. We can see that the

Table 1
Grid independence study with $A = 0.5$, $Ra_T = 0$, $Sc = 1$, $Pe = 10$ and $Ra = 10^3$

$N_x \times N_y$	26×26	51×101	76×151	101×201
ψ_{max}	0.2861	0.2862	0.2873	0.2870
n_{max}	13.396	11.771	11.580	11.466

variation in the last two cases is less than 1×10^{-3}, which is negligibly small. Hence, the results presented here are obtained with 51×51 grid size for $A = 1$, 51×101 for $A = 0.5$ and 51×251 for $A = 0.2$, and all with $\Delta t = 0.01$ and $\varepsilon = 10^{-6}$.

We validated the code earlier [21], which is summarized here. Eqs. (5)–(7) with $Ra_T = 0$ and boundary conditions Eqs. (9)–(12) possess a steady state solution for which $\psi = \omega = 0$. We solved them analytically and compared the results to those obtained numerically using the present code (not presented here). The agreement found was excellent for $Pe = 1$ and 10. Additionally, as we will present later, by using the present code, we simulated the Rayleigh–Bénard convection in a horizontal fluid layer heated from below by constant heat flux and produced the bifurcation diagram. We determined the critical Rayleigh number as 1708, which is consistent with the literature [22].

The code was validated also with the case of double diffusion for $A = 1.5$, $Ra_T = 40{,}000$, $Ra_s = -10^5$, $Pr = 1$, $Le = 10^{1/2}$, which showed that the present code reproduced exactly the same iso-patterns of Q, T and S, and very good

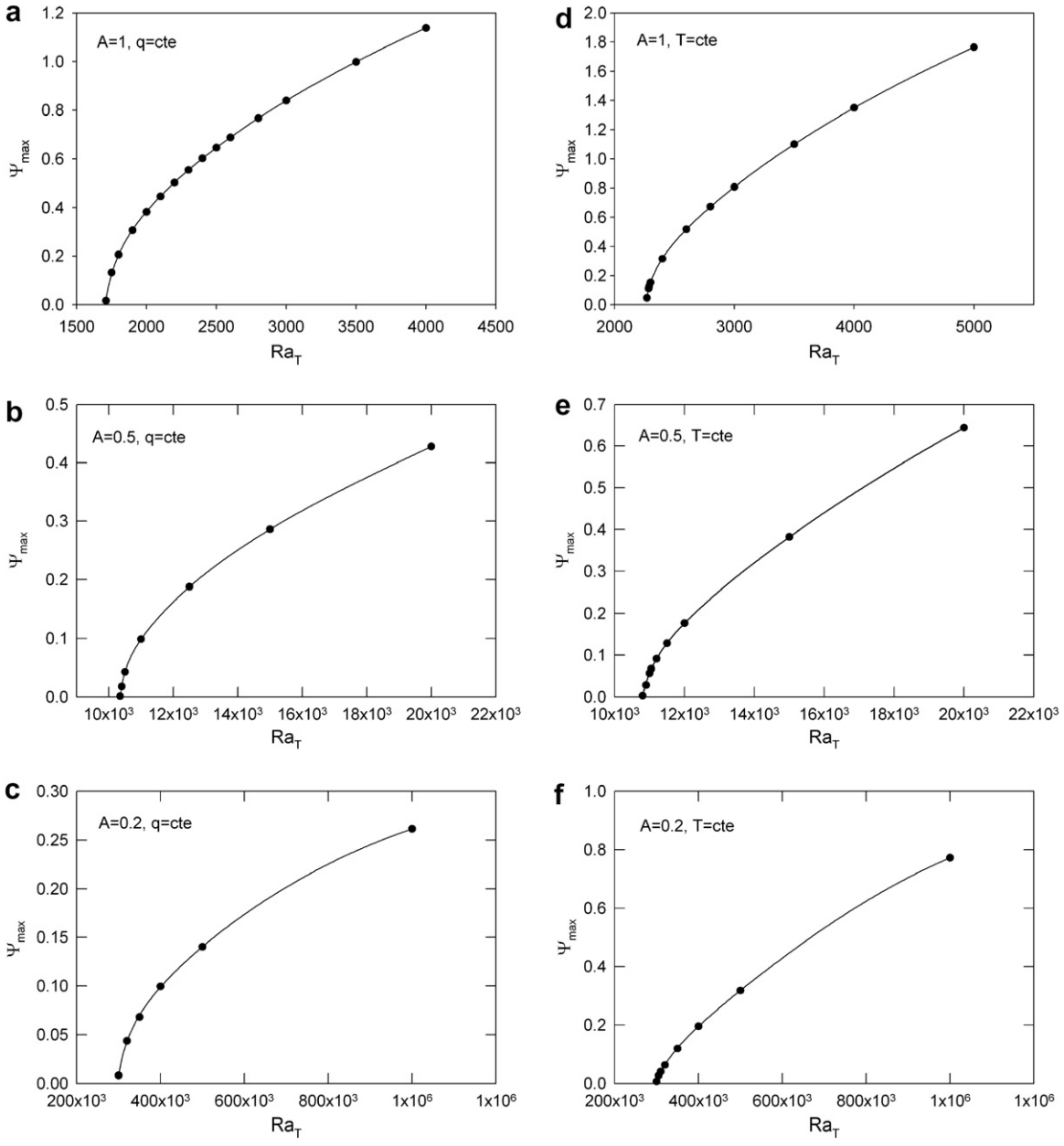

Fig. 2. Bifurcation diagrams for thermo-convection, $Ra = 0$ (no bioconvection): (a) $A = 1$, $T =$ constant, (b) $A = 0.5$, $T =$ constant, (c) $A = 0.2$, $T =$ constant, (d) $A = 1$, $q =$ constant, (e) $A = 0.5$, $q =$ constant, and (f) $q = 0.2$, $q =$ constant.

agreement for ψ_{max}, ψ_{min}, as well as for Nusselt and Sherwood numbers, Nu_m and Sh_m [19].

4. Results and discussion

Computations were performed with the aspect ratio of $A = 1$, 0.5, 0.2 and variable Ra_T and Ra for the following values of dimensionless parameters: $Sc = 1$, $Le = 1$, $Pe = 1$ and 10, which correspond to typical bioconvection cases with known micro-organism characteristics (e.g. [23,24]). First, we obtained bifurcation curves by numerical simulation, the critical thermal Rayleigh numbers, Ra_{Tc} without bioconvection, i.e. with $Ra = 0$. Then, we obtained bifurcation curves by numerical simulation, the subcritical bioconvection Rayleigh numbers, Ra_c without thermal effect, i.e. with $Ra_T = 0$. Finally, by using the critical thermal Rayleigh numbers and the subcritical bioconvection Rayleigh numbers, we studied by numerical simulation to obtain bifurcation curves to determine the critical Rayleigh numbers at $Ra_T = 1 \times Ra_{Tc}$, $2 \times Ra_{Tc}$ (i.e. heating from below) and $Ra_T = -1 \times Ra_{Tc}$, $-2 \times Ra_{Tc}$ (i.e. cooling from below) using the conditions of $T =$ constant and $q =$ constant.

Fig. 2 displays the bifurcation diagrams (ψ_{max} vs. Ra_T) for the case of thermal convection, i.e. no bioconvection, $Ra = 0$, for heating from the bottom at isothermal and constant heat flux. A bifurcation between purely conductive and convective states is clearly seen in Fig. 2a–c at $Ra_{Tc} = 1708$, 10, 350 and 298×10^3 for $A = 1$, 0.5 and 0.2, respectively. They are the critical Rayleigh numbers of a horizontal fluid layer in a vertical cylinder heated from below at constant heat flux. Similarly we see in Fig. 2d–f the bifurcations at $Ra_{Tc} = 2265$, 10, 800 and 299.4×10^3,

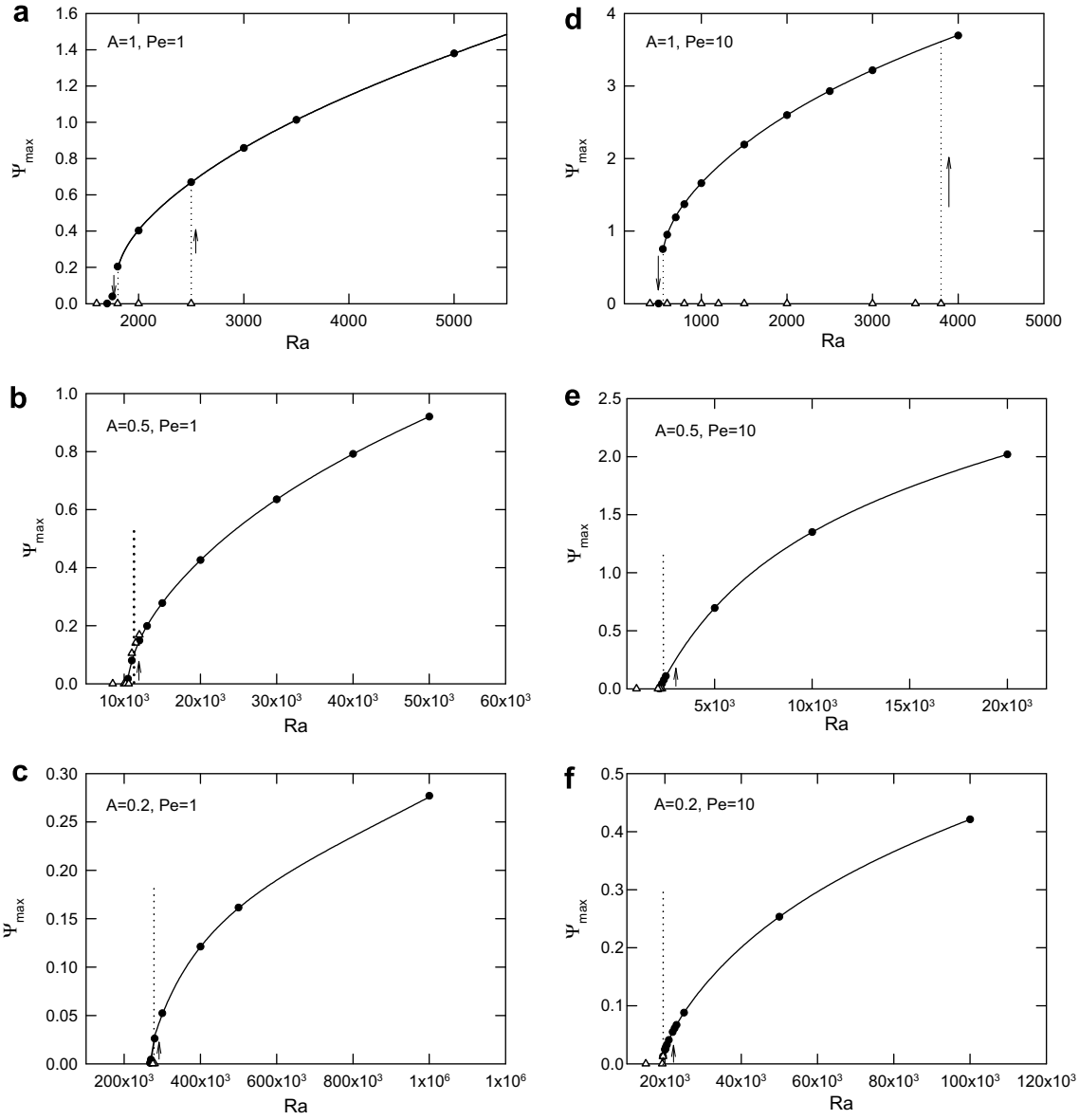

Fig. 3. Bifurcation diagrams for bioconvection, $Ra_T = 0$ (no thermal effect). (a) $A = 1$, $Pe = 1$, (b) $A = 0.5$, $Pe = 1$, (c) $A = 0.2$, $Pe = 1$, (d) $A = 1$, $Pe = 10$, (e) $A = 0.5$, $Pe = 10$, and (f) $A = 0.2$, $Pe = 10$.

which are the critical Rayleigh numbers when heated from below at constant temperature. Fig. 2a–c correspond to the classical Rayleigh–Bénard problem [22].

Fig. 3 shows the bifurcation diagrams (ψ_{ext} vs. Ra) for the case of isothermal cavity, i.e. at $Ra_T = 0$. These results are obtained by beginning the simulation at a high Rayleigh number, which is estimated by trial and error to have a convection state. We obtained solutions at lower Rayleigh numbers using the solution at the previous, higher Rayleigh number as initial condition. Then, we started with the diffusion state (i.e. no convection) as initial condition, gradually increasing the Rayleigh number until convection arises. As usual, at each step we continued to obtain solutions at higher Rayleigh numbers by initializing using the solution at the previous, lower Rayleigh number. Thus, we determined the supercritical Rayleigh numbers.

We see that the bifurcations are all subcritical with bioconvection Rayleigh numbers, Ra_c^{sub}, which are obtained for the cases of a horizontal fluid layer in a vertical cylinder for $Pe = 1$ in Fig. 3a–c and for $Pe = 10$ in Fig. 3d–f. The subcritical bioconvection Rayleigh numbers for $Pe = 1$ are $Ra_c^{sub} = 1710$, 10,400 and 270×10^3 for $A = 1$, 0.5 and 0.2, respectively. For $Pe = 10$, they are $Ra_c^{sub} = 520$, 2160 and 19,000 for $A = 1$, 0.5 and 0.2, respectively. We note that the subcritical bioconvection Rayleigh number is higher for smaller bioconvection Peclet number. The same phenomenon was also observed earlier [21]. We note also that for the aspect ratio of $A = 1$, the unstable region between Ra_c^{sub} and Ra_c^{sup} is quite distinct. Yet, for $A = 0.5$ and 0.2 it is almost merged. For example, for $A = 0.5$ and $Pe = 1$, $Ra_c^{sub} = 10,400$ and $Ra_c^{sup} = 11,000$, and for $A = 0.5$ and $Pe = 10$, $Ra_c^{sub} = 2160$ and $Ra_c^{sup} = 2350$; for $A = 0.2$ and $Pe = 1$, $Ra_c^{sub} = 269,000$ and $Ra_c^{sup} = 280,000$ and for $A = 0.2$ and $Pe = 10$, $Ra_c^{sub} = 19,100$ and $Ra_c^{sup} = 19,500$.

We studied the effect of heating and cooling from below at constant temperature and constant heat flux with $Pe = 1$ and 10, and the aspect ratio of $A = 1$, 0.5 and 0.2. We obtained bifurcation diagrams with $Ra_T = 1 \times Ra_{Tc}$ and $2 \times Ra_{Tc}$ (i.e. corresponding to heating from below) and $Ra_T = -1 \times Ra_{Tc}$ and $-2 \times Ra_{Tc}$ (i.e. corresponding to cooling from below) at constant temperature and constant heat flux; the critical thermal Rayleigh numbers employed here, Ra_{Tc} are those obtained for heating from below at constant temperature and constant heat flux and presented in Fig. 2. The procedure was to use a starting Rayleigh number, $Ra \geqslant 5 \times Ra_c$ and after obtaining the first solution, continue to obtain a new solution at a lower Ra by using the previous solution at higher Ra as initial condition. We continued the same procedure until we obtained diffusive state.

Bifurcation results are shown in Fig. 4a–c for $Pe = 1$ and Fig. 5a–c for $Pe = 10$. Each figure shows the bifurcation diagrams for heating and cooling from below with constant temperature (shown with dashed lines) and constant heat flux (shown with full lines) for $A = 1$, 0.5 and 0.2 in figures (a), (b) and (c), respectively. In addition,

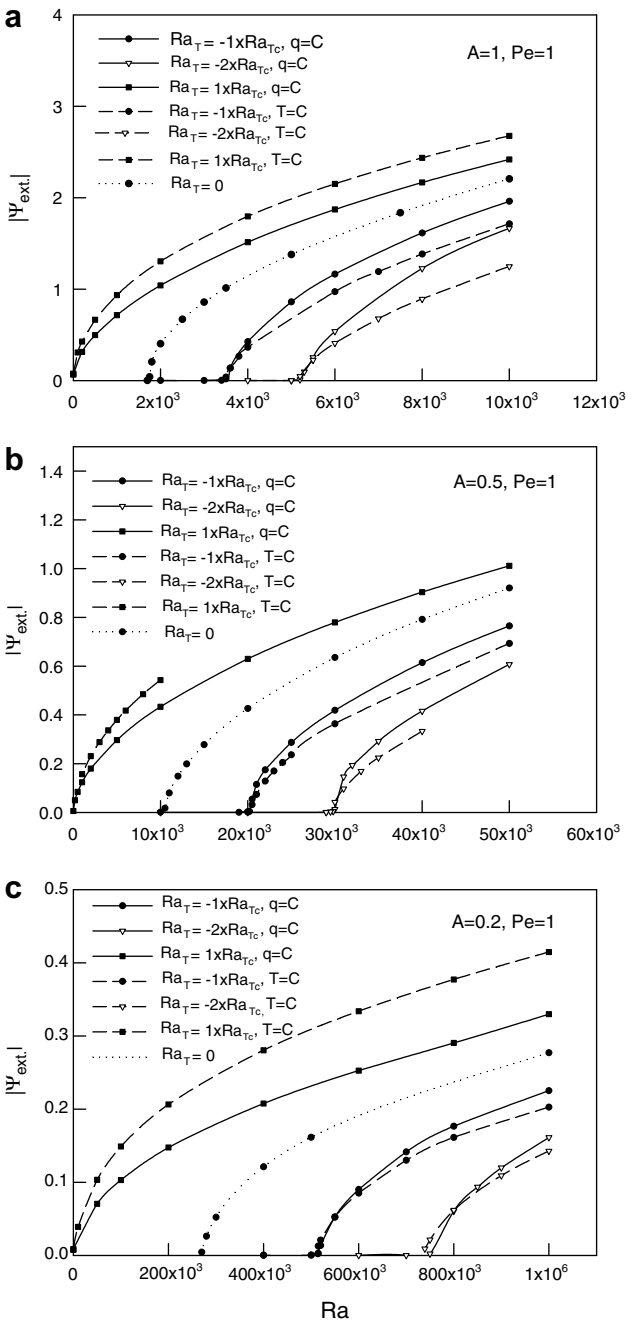

Fig. 4. Bifurcation diagrams for thermo-bioconvection, $Ra_T = -1 \times Ra_{Tc}$, $-2 \times Ra_{Tc}$, $1 \times Ra_{Tc}$ and $Pe = 1$: (a) $A = 1$, (b) $A = 0.5$, and (c) $A = 0.2$.

the bifurcation curve for $Ra_T = 0$, i.e. the bioconvection bifurcation curve for a given A is also included in the same figure for the same aspect ratio A as reference.

Generally, in all bifurcations the extremum stream function ψ_{ext} is smaller at a given Rayleigh number when the fluid layer is cooled from below by a constant temperature or constant heat flux with respect to that of the bioconvection only. Thus, we see in Fig. 4a–c that the bifurcation diagrams fall below the bioconvection bifurcation diagram and the critical Rayleigh numbers are higher. This case

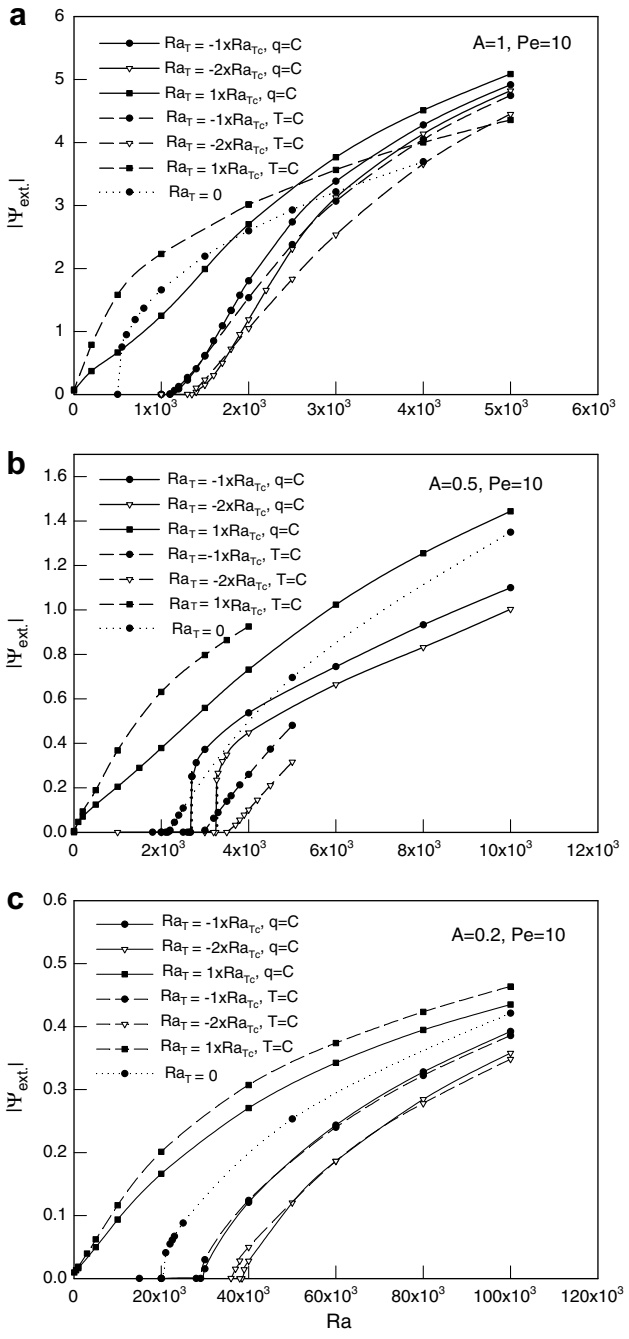

Fig. 5. Bifurcation diagrams for thermo-bioconvection, $Ra_T = -1 \times Ra_{Tc}$, $-2 \times Ra_{Tc}$, $1 \times Ra_{Tc}$ and $Pe = 10$: (a) $A = 1$, (b) $A = 0.5$, and (c) $A = 0.2$.

represents opposing buoyancy forces and the resulting convection is reduced. The convection is reduced more when the cooling from below is by a constant temperature. Another striking result is that the critical Rayleigh numbers obtained by cooling from below by constant temperature and constant heat flux are the same.

In contrast, the extremum stream function ψ_{ext} at a given Rayleigh number is higher than that of bioconvection when the fluid layer is heated from below. This case corresponds to cooperating buoyancy forces and the resulting convection is enhanced. The convection is higher when heated from below at constant temperature than at constant heat flux. Similar to the case of cooling from below, the critical Rayleigh numbers for this case with $Ra_T = 1 \times Ra_{Tc}$ for heating at constant temperature and constant heat flux are the same and equal to zero, as they should be, since $Ra_T = Ra_{Tc}$. However, at $Ra_T = 2 \times Ra_{Tc}$ we could not obtain critical Rayleigh numbers, hence no bifurcation. Indeed, for this case of heating at constant temperature and constant heat flux, we checked starting from diffusion state, i.e. initializing at uniform temperature and concentration and obtained convection only. This shows that the cooperating thermal buoyancy forces are too strong and a diffusion state does not exist. We present ψ_{ext} obtained at $Ra = 0$ and its coordinates in Table 2 for $Ra_T = 2 \times Ra_{Tc}$, i.e. heated from below at constant temperature and at constant heat flux, and for various aspect ratios. We see in this table that ψ_{ext} (r, z) is identical for $Pe = 1$ and 10 for a given aspect ratio. The isolines of ψ_{ext}, n and T showed (not presented here) that for $A = 1$ and 0.5, there was a single clockwise rotating convection cell. The isotherms and isoconcentration lines showed similar trends with micro-organisms concentration at the top corner, near $r = A$ when heated from below at constant heat flux and at the center, near $r = 0$ when heated from below at constant temperature. We note that at $Ra = 0$, there is no bioconvection and the concentration of micro-organisms at the top is as a result of thermal convection. For $A = 0.2$, similar observations were made when heated from below at constant temperature but there were two symmetrical convection cells with respect to the mid-plane when heated from below at constant heat flux. Consequently, isotherms and isoconcentration lines were also similarly symmetric with respect to the mid-plane. We see in Fig. 4a–c that the effect of increasing aspect ratio on the critical Rayleigh number is to increase it.

We see in Fig. 5a–c that the effect of heating and cooling from below is relatively higher for $Pe = 10$ than for $Pe = 1$ since the strength of the bioconvection is relatively higher

Table 2
ψ_{ext} and its coordinates for $Ra_T = 2 \times Ra_{Tc}$ at $Ra = 0$

Aspect ratio, A	Pe	Thermal boundary condition	Ra_T	ψ_{ext}	(r, z)
1	1	q = constant	2×1710	0.9821	(0.58, 0.56)
		T = constant	2×2270	1.5893	(0.58, 0.42)
	10	q = constant	2×1710	0.9821	(0.58, 0.56)
		T = constant	2×2270	1.5893	(0.58, 0.42)
0.5	1	q = constant	$2 \times 10{,}350$	0.4450	(0.28, 0.34)
		T = constant	$2 \times 10{,}800$	0.6489	(0.28, 0.32)
	10	q = constant	$2 \times 10{,}350$	0.4450	(0.28, 0.34)
		T = constant	$2 \times 10{,}800$	0.6489	(0.28, 0.32)
0.2	1	q = constant	$2 \times 298{,}000$	0.1466	(0.11, 0.845)
		T = constant	$2 \times 299{,}400$	0.4306	(0.11, 0.135)
	10	q = constant	$2 \times 298{,}000$	0.1466	(0.11, 0.845)
		T = constant	$2 \times 299{,}400$	0.4306	(0.11, 0.135)

in the former case. The reason is that Pe is non-dimensional swimming velocity of micro-organisms in opposing direction to the gravity as well as thermal diffusion forces in case of cooling from below. It is in the same direction in case of heating from below. Thus, we will have opposing forces in play in case of cooling from below and cooperating forces in case of heating from below. Indeed, we see in Fig. 5a–c that as expected, with all three aspect ratios $Ra_{Tc} = 0$ at $Ra = 0$ for $Ra_T = 1 \times Ra_{Tc}$. Generally, for the opposing buoyancy case, i.e. cooling from below, convection is lower than that for bioconvection only. It is the reverse in the cooperating buoyancy case, i.e. heating from below. In case with $Ra_T = 2 \times Ra_{Tc}$ in heating from below at constant temperature and constant heat flux, we observed the same phenomenon of sudden convection starting from diffusion state at $Ra = 0$. For this case ψ_{ext} obtained at $Ra = 0$ and its coordinates are also shown in Table 2. We see that ψ_{ext} and their coordinates are the same as for $Pe = 1$. The reason is, as discussed before, because there is no bioconvection at $Ra = 0$. By examining the isolines for this case we noticed that they were all identical to those for $Pe = 1$ except isoconcentration lines. They showed almost total accumulation of micro-organisms at the top right corner, near $r = A$ when heated from below at constant heat flux and at the center, near $r = 0$ when heated from below at constant temperature. We see in Fig. 5a and c that in case of $A = 1$ and 0.2, as observed earlier with $Pe = 1$ in Fig. 4, the critical Rayleigh numbers are the same or almost the same for cooling from below at constant temperature and at constant heat flux. However, they are not the same in case of $A = 0.5$ in Fig. 5b. In this case, the critical Rayleigh number is higher for cooling from below at constant temperature than at constant heat flux. To see the reason, we produced isolines ψ, n, T at near critical Rayleigh numbers for the cases of constant temperature and heat flux, all for cooling from below and presented in Fig. 6a–d. For the case with $Ra_T = -1 \times Ra_{Tc}$, and $Ra = 3000$ and 2700 for constant temperature or heat flux, respectively in Fig. 6a and c, we see that all three isolines are quite different: a single convection cell circulated clockwise when cooling from below at constant temperature, ψ_{ext} is 0.009 at $Ra = 3000$, i.e. almost a diffusive state, the micro-organisms are accumulated almost uniformly at the top and the isotherms show a conduction regime. For cooling from below at constant heat flux in Fig. 6c, a single cell circulates counterclockwise, ψ_{ext} is -0.25 at $Ra = 2700$, the micro-organisms are accumulated at the top, near $r = 0$ and the isotherms show a conduction regime with negative values at the bottom, positive values at the top. The case with $Ra_T = -2 \times Ra_{Tc}$ for both cooling from below at constant temperature and at constant heat flux is quite similar to the case with $Ra_T = -1 \times Ra_{Tc}$. At Ra = 3700 and 3270 for T or q constant, respectively, in Fig. 6b and d, corresponding ψ_{ext} is 0.033 and -0.235 and isolines for concentration and temperature are almost identical to those with $Ra_T = -1 \times Ra_{Tc}$. In contrast, we found identical isolines in the other cases with identical critical

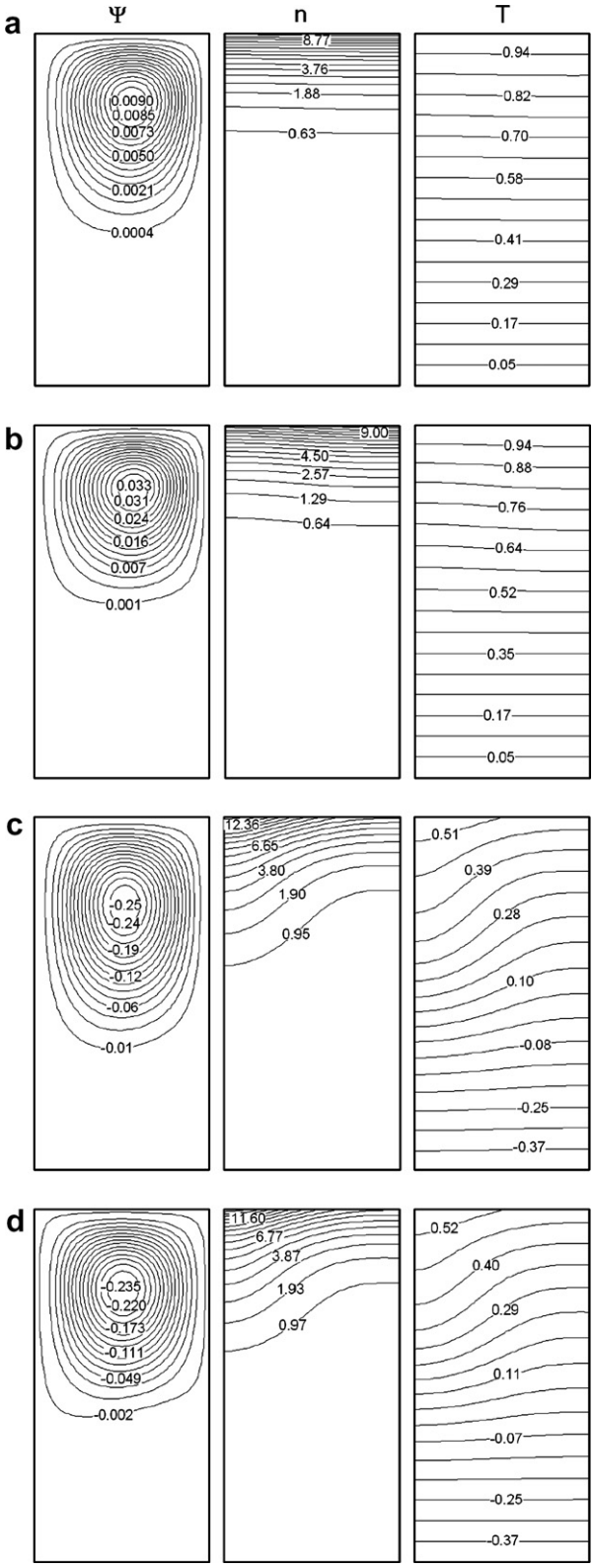

Fig. 6. Streamlines, isoconcentration and isotherms for thermo-bioconvection, $A = 0.5$, $Pe = 1$ and at near critical Rayleigh numbers: (a) T = constant, $Ra_T = -1 \times Ra_{Tc}$ (b) T = constant, $Ra_T = -2 \times Ra_{Tc}$ (c) q = constant, $Ra_T = -1 \times Ra_{Tc}$, and (d) q = constant, $Ra_T = -2 \times Ra_{Tc}$.

Rayleigh numbers for cooling from below at constant temperature or heat flux. Thus, we conclude that the reason for

different critical Rayleigh numbers obtained in Fig. 5b could be an aspect ratio effect.

The onset of bioconvection with $Ra_T = 0$ is subcritical in all cases as shown in Fig. 3 and it is transposed also in Figs. 4 and 5. At Ra_T from $-2 \times Ra_{Tc}$ to $+2 \times Ra_{Tc}$, the effect of the thermal Rayleigh number is to increase or decrease the convection, because the buoyancy forces developed are either cooperating or opposing the bioconvection. We see that for all cases considered in this study, the thermal effect Ra_T on the onset of the bioconvection is to make the subcritical bioconvection strongly supercritical.

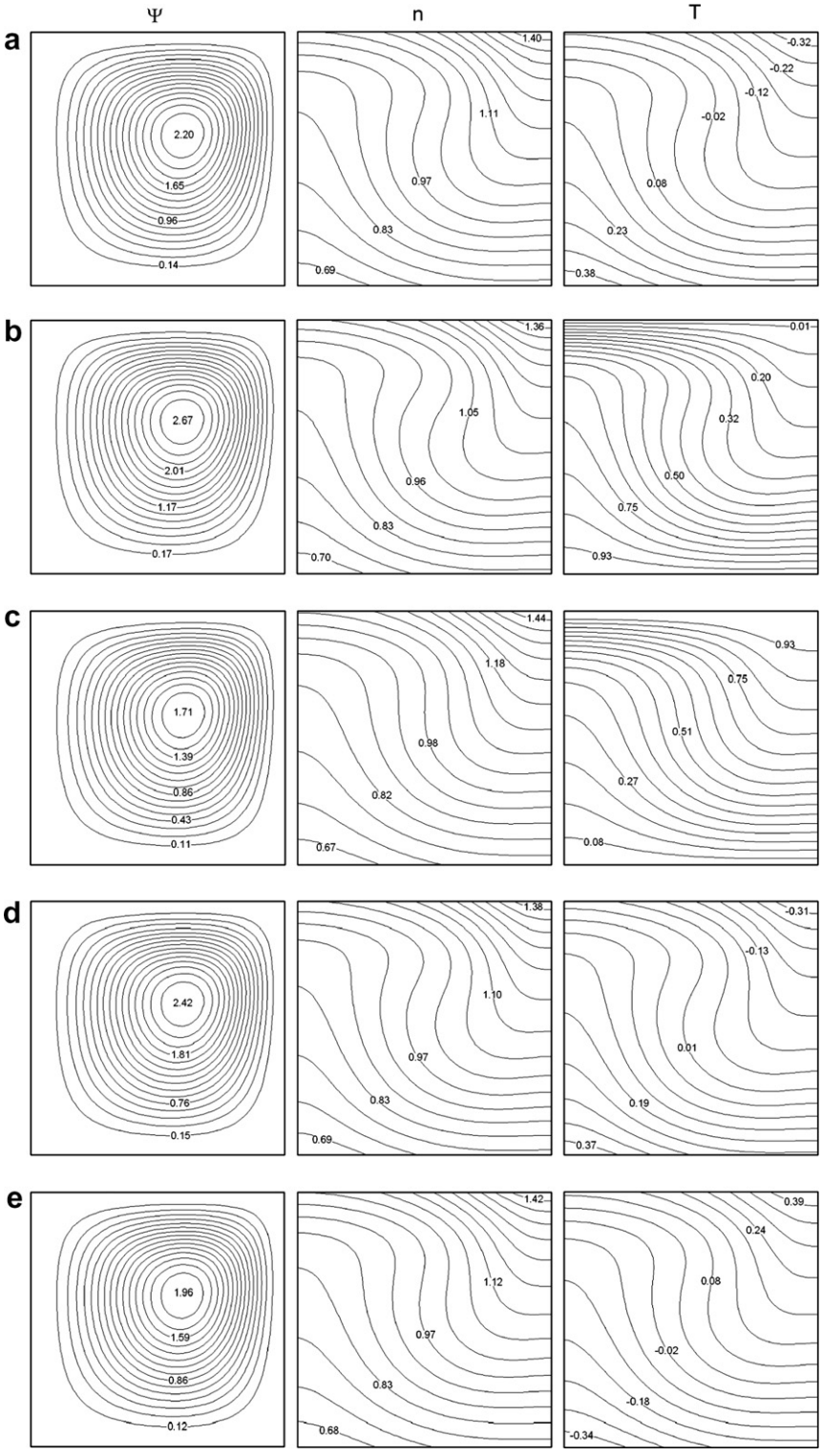

Fig. 7. Streamlines, isoconcentration and isotherms for $A = 1$, $Pe = 1$ and $Ra = 5 \times Ra_c$: (a) $Ra_T = 0$ (b) $T =$ constant, $Ra_T = 1 \times Ra_{Tc}$ (c) $T =$ constant, $Ra_T = -1 \times Ra_{Tc}$ (d) $q =$ constant, $Ra_T = 1 \times Ra_{Tc}$, and (e) $q =$ constant, $Ra_T = -1 \times Ra_{Tc}$.

To examine the flow, concentration and temperature patterns at $Ra = 5 \times Ra_c$, streamlines and isoconcentration of selected cases at $Ra_T = 1 \times Ra_{Tc}$, $-1 \times Ra_{Tc}$ of Figs. 4 and 5 are plotted in Figs. 7–9, for $A = 1$, 0.5 and 0.2, respectively.

We present the case with $A = 1$, $Pe = 1$, $Ra = 5 \times Ra_c$ in Fig. 7a–e. The case of bioconvection with $Ra_T = 0$ is shown as reference in (a), the circulation of convection cell is clockwise and $\psi_{ext} = 2.20$. The convection cell is slightly asymmetric and transports the micro-organisms towards the upper corner near $r = A$. The cases with constant temperature heating and cooling are presented in Fig. 7b and c. For $Ra_T = 1 \times Ra_{Tc}$, i.e. heating from below at constant temperature in Fig. 7b, the thermal buoyancy forces are cooperating and the strength of convection is increased to $\psi_{ext} = 2.67$. The concentration isolines are similar to those for bioconvection. The isotherms show high temperature gradients at the top center, near $r = 0$. For $Ra_T = -1 \times Ra_{Tc}$, and for cooling from below at constant temperature in Fig. 7c, the thermal buoyancy forces are opposing and the strength of convection is decreased to $\psi_{ext} = 1.71$. The concentration isolines are similar to those in case of b. As expected, the isotherms show that temperature gradients at the top center, near $r = 0$ slightly reduced. We present the cases for heating and cooling at constant heat flux in Fig. 7d and e. For $Ra_T = 1 \times Ra_{Tc}$, i.e. heating from below at constant heat flux in Fig. 7d, the thermal buoyancy forces are cooperating and the strength of convection is increased to $\psi_{ext} = 2.42$, which is slightly reduced with respect to that for heating from below at constant temperature in (b), though the concentration isolines are very similar. As expected, the isotherms are completely different with lower temperature gradients changing sign at approximately mid-plane. At $Ra_T = -1 \times Ra_{Tc}$, and for cooling from below at constant heat flux in Fig. 7e, the thermal buoyancy forces are opposing and the strength of convection is decreased to $\psi_{ext} = 1.96$, lower than that for bioconvection in (a) but higher than that in (c). The concentration isolines and the isotherms are similar to those in case (d).

We present ψ_{ext}, n, T for $A = 0.5$, $Pe = 1$, $Ra = 5 \times Ra_c$ in Fig. 8a–d. The cases (a) and (b) are for heating and cooling below at constant temperature and (c) and (d) for heating and cooling from below at constant heat flux. We note that the bioconvection in this case (not shown here), had a single counterclockwise circulating convection cell with $\psi_{ext} = -0.92$ and the micro-organisms accumulated at the top center, near $r = 0$. We see in Fig. 8a that for $Ra_T = 1 \times Ra_{Tc}$, the single convection cell is circulating counterclockwise, almost symmetric. Its strength is $\psi_{ext} = -1.15$. Due to its circulation direction, the micro-organisms are concentrated at the center, near $r = 0$. As expected, the isotherms show high temperature gradients at the bottom and on the top right side. For $Ra_T = -1 \times Ra_{Tc}$ in Fig. 8b, i.e. in cooling from below at constant temperature, in contrast to that of Fig. 7a, the circulation of the single convection cell is clockwise and the circulation strength is reduced to $\psi_{ext} = 0.73$, because of opposing thermal buoyancy forces.

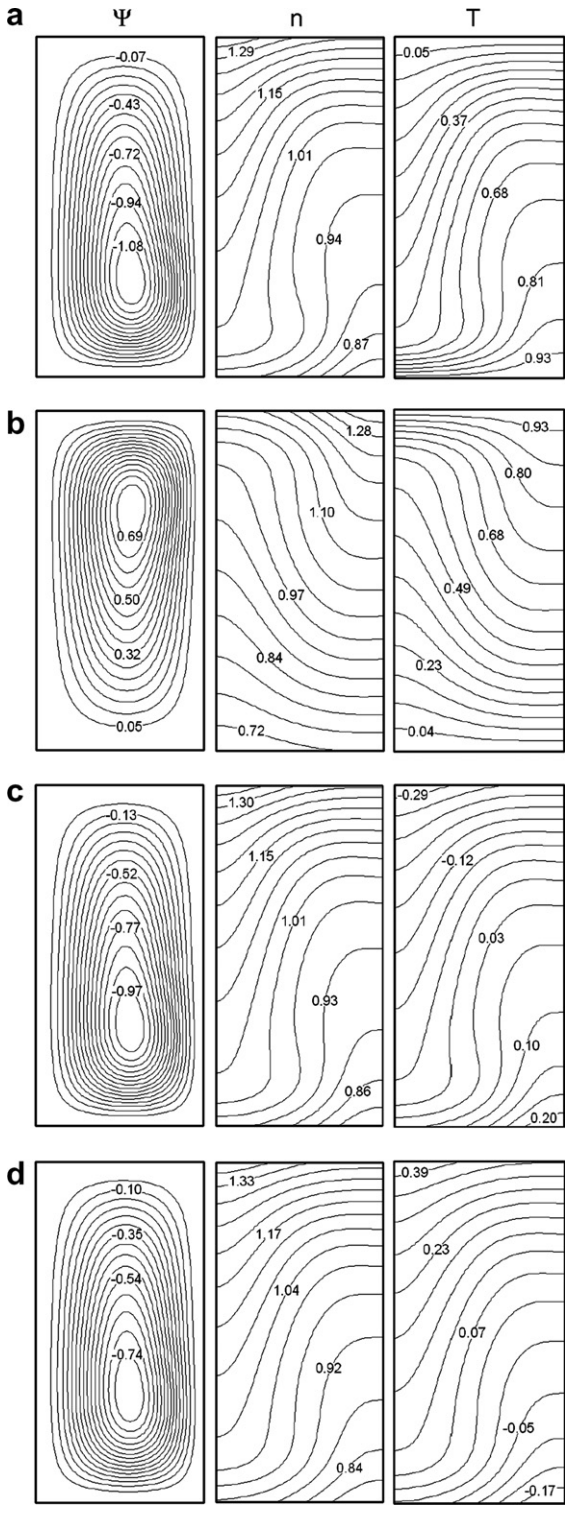

Fig. 8. Streamlines, isoconcentration and isotherms for thermo-bioconvection, $A = 0.5$, $Pe = 1$ and $Ra = 5 \times Ra_c$: (a) T = constant, $Ra_T = 1 \times Ra_{Tc}$, (b) T = constant, $Ra_T = -1 \times Ra_{Tc}$, (c) q = constant, $Ra_T = 1 \times Ra_{Tc}$, and (d) q = constant, $Ra_T = -1 \times Ra_{Tc}$.

The isoconcentration and isotherms are almost a mirror image of those in (a).

The results for heating and cooling from below at constant heat flux are presented in Fig. 8c and d. For

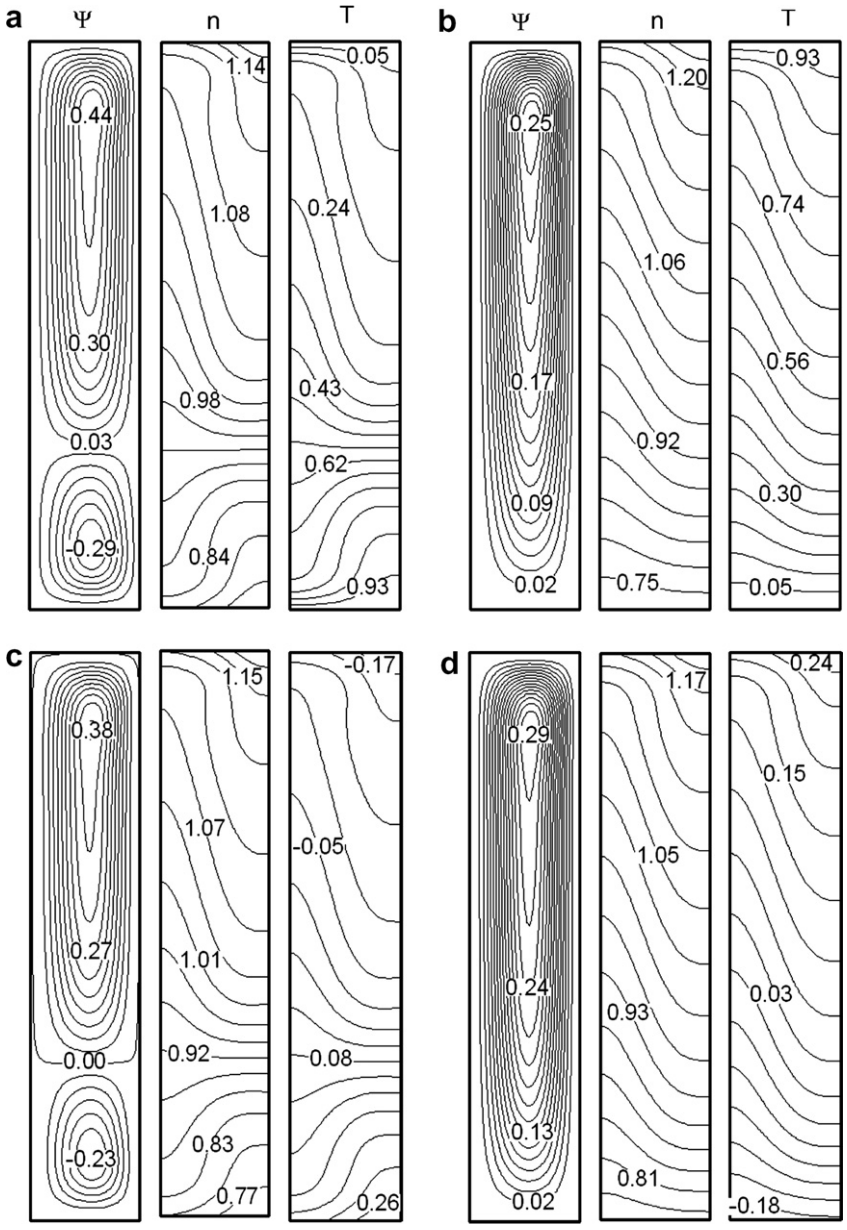

Fig. 9. Streamlines, isoconcentration and isotherms for thermo-bioconvection, $A = 0.2$, $Pe = 1$ and $Ra = 5 \times Ra_c$: (a) $T =$ constant, $Ra_T = 1 \times Ra_{Tc}$, (b) $T =$ constant, $Ra_T = -1 \times Ra_{Tc}$, (c) $q =$ constant, $Ra_T = 1 \times Ra_{Tc}$, and (d) $q =$ constant, $Ra_T = -1 \times Ra_{Tc}$.

$Ra_T = 1 \times Ra_{Tc}$ in Fig. 8c, we have a counterclockwise circulating single convection cell with a circulation strength of $\psi_{ext} = -1.03$. Consequently the micro-organisms are concentrated at the center near $r = 0$. Both streamlines and isoconcentration lines are similar to the case with constant temperature. The isotherms are with smaller temperature gradients, positive at the bottom and negative at the top, a typical characteristic of constant heat flux case. For $Ra_T = -1 \times Ra_{Tc}$ in Fig. 8d, i.e. cooling from below at constant heat flux, the flow and concentration fields as well as the isotherms are similar to those in (c) but the circulation strength is reduced to $\psi_{ext} = -0.79$, the concentration at the top is slightly increased and the isotherms are positive at the top and negative at the bottom. We note that in this case, we still have a counterclockwise circulation and for this reason the pattern did not change with respect to the case (c).

We present ψ_{ext}, n, T for $A = 0.2$, $Pe = 1$, $Ra = 5 \times Ra_c$ in Fig. 9a–d. Heating and cooling from below at constant temperature are in Fig. 9a and b and those at constant heat flux in Fig. 9c and d. We note that for bioconvection in this case (not shown here), we had two convection cells, the lower one in counterclockwise circulation with $\psi_{ext} = -0.16$ and the upper one in clockwise circulation with $\psi_{ext} = 0.34$. The micro-organisms were accumulated at the top right corner with some stratification in the enclosure. For $Ra_T = 1 \times Ra_{Tc}$, i.e. heating from below in Fig. 9a, we have two counter rotating cells, the lower one counterclockwise circulating with $\psi_{ext} = -0.29$ and the clockwise circulating upper one with $\psi_{ext} = 0.44$. Following

circulation direction, the micro-organisms are concentrated mainly on the top right corner, near $r = A$, and the isotherms show high temperature gradients at bottom and top center. The appearance of flow and concentration fields is exactly similar to those for bioconvection with increased strength. For $Ra_T = -1 \times Ra_{Tc}$, i.e. cooling from below, in Fig. 9b, a single clockwise circulating convection cell fills the cavity with $\psi_{ext} = 0.25$. The isoconcentration as well as the isotherms are quasi-stratified. Following circulation direction, the micro-organisms concentration is highest at the top right corner.

The case with heating and cooling at constant heat flux is presented in Fig. 9c and d. For $Ra_T = 1 \times Ra_{Tc}$, i.e. heating from below, in Fig. 9c, similar to that in (a), we have two counter rotating cells, the lower one counterclockwise circulating with $\psi_{ext} = -0.23$ and the clockwise circulating upper one with $\psi_{ext} = 0.38$. Patterns of isoconcentration lines and isotherms are very similar to those in Fig. 9a, except the isotherms are positive on the bottom corresponding to the counterclockwise rotating cell and negative on the top corresponding to the clockwise rotating cell. For $Ra_T = -1 \times Ra_{Tc}$, i.e. cooling from below, in Fig. 9d, the patterns are similar to those in (b) with a single clockwise circulating convection cell filling the cavity with the circulation strength reduced to $\psi_{ext} = 0.29$. The isoconcentration as well as the isotherms are quasi-stratified. Following circulation direction, the micro-organisms concentration is highest at the top right corner. Similar to the case in (c), the isotherms are in this case negative at the bottom and positive in the upper part.

5. Conclusion

Numerical simulations of thermo-bioconvection in vertical cylinders are carried out. The vertical walls of the cavity are assumed to be stress free and insulated, while horizontal boundaries are rigid. For heating and cooling from below at constant temperature, the horizontal boundaries were maintained at fixed temperatures. For heating and cooling from below at constant heat flux, constant heat fluxes through the horizontal boundaries were maintained. The governing equations are integrated numerically using the control volume method.

The results show the influence of thermal effect on the bifurcation diagram and the pattern of gravitactic bioconvection. We found that subcritical bifurcations of bioconvection became supercritical when the thermal Rayleigh number Ra_T is different than zero. For $Ra_T < 0$, i.e. for cooling from below, we have opposing buoyancy forces, the convection is decreased, the concentration isolines are modified to reflect the change in the flow field, and the critical thermo-bioconvection Rayleigh number is increased with respect to that of bioconvection. For $Ra_T > 0$, i.e. for heating from below, we have cooperating buoyancy forces, the convection is increased, the concentration isolines are changed, and the critical thermo-bioconvection Rayleigh number is decreased with respect to that of bioconvection. We found that the pattern formation of the gravitactic bioconvection is considerably modified when heating and cooling from below at constant temperature and constant heat flux.

Acknowledgement

The financial support for this study by Natural Sciences and Engineering Research Council Canada is acknowledged.

References

[1] S. Childress, M. Levandowsky, E.A. Spiegel, Pattern formation in a suspension of swimming micro-organisms: equations and stability theory, J. Fluid Mech. 63 (1975) 591–613.
[2] J.O. Kessler, Gyrotactic buoyant convection and spontaneous pattern formation in algal cell cultures, in: M.G. Velarde (Ed.), Non-equilibrium Cooperative Phenomena in Physics and Related Fields, Plenum, New York, 1984, pp. 241–248.
[3] A.J. Hillesdon, T.J. Pedley, J.O. Kessler, The development of concentration gradients in a suspension of chemotactic bacteria, Bull. Math. Biol. 57 (2) (1995) 299–344.
[4] J.O. Kessler, The external dynamics of swimming micro-organisms, in: F.E. Round, D.J. Chapman (Eds.), Progress in Physiological Research, vol. 4, Bristol Biopress, 1986, pp. 257–307.
[5] T.J. Pedley, J.O. Kessler, Hydrodynamic phenomena in suspensions of swimming micro-organisms, Ann. Rev. Fluid Mech. 24 (1992) 313–358.
[6] N.A. Hill, T.J. Pedley, Bioconvection, Fluid Dyn. Res. 37 (2005) 1–20.
[7] S. Fujita, M. Watanabe, Transition from periodic to non-periodic oscillation observed in a mathematical model of bioconvection by motile micro-organisms, Phys. D: Nonlinear Phenom. 20 (1986) 435–443.
[8] A. Harashima, M. Watanabe, L. Fujishiro, Evolution of bioconvection patterns in a culture of motile flagellates, Phys. Fluids 31 (1988) 764–775.
[9] S. Ghorai, N.A. Hill, Development and stability of gyrotactic plumes in bioconvection, J. Fluid Mech. 400 (1999) 1–31.
[10] S. Ghorai, N.A. Hill, Wavelengths of gyrotactic plumes in bioconvection, Bull. Math. Biol. 62 (2000) 429–450.
[11] S. Ghorai, N.A. Hill, Periodic arrays of gyrotactic plumes in bioconvection, Phys. Fluids 12 (2000) 5–22.
[12] S. Ghorai, N.A. Hill, Axisymmetric bioconvection in a cylinder, J. Theor. Biol. 219 (2002) 137–152.
[13] T.J. Pedley, N.A. Hill, J.O. Kessler, The growth of bioconvection patterns in a uniform suspension of gyrotactic micro-organisms, J. Fluid Mech. 195 (1988) 223–237.
[14] A.V. Kuznetsov, The onset of bioconvection in a suspension of gyrotactic micro-organisms in a fluid layer of finite depth heated from below, Int. Commun. Heat Mass Trans. 32 (2005) 574–582.
[15] A.V. Kuznetsov, Thermo-bioconvection in a suspension of oxytactic bacteria, Int. Commun. Heat Mass Trans. 32 (2005) 991–999.
[16] A.V. Kuznetsov, Investigation of the onset of thermo-bioconvection in a suspension of oxytactic micro-organisms in a shallow fluid layer heated from below, Theor. Comput. Fluid Dyn. 19 (2005) 287–299.
[17] D.A. Nield, A.V. Kuznetsov, The onset of bio-thermal convection in a suspension of gyrotactic micro-organisms in a fluid layer: oscillatory convection, Int. J. Therm. Sci. 45 (2006) 990–997.
[18] Z. Alloui, T.H. Nguyen, E. Bilgen, Stability analysis of thermo-bioconvection in suspensions of gravitactic micro-organisms in a fluid layer, Int. Commun. Heat Mass Trans. 33 (2006) 1198–1206.

[19] Z. Alloui, T.H. Nguyen, E. Bilgen, Numerical investigation of thermo-bioconvection in a suspension of gravitactic micro-organisms, Int. J. Heat Mass Trans. 50 (2007) 1439–1441.
[20] S.V. Patankar, Numerical Heat Transfer and Fluid Flow, McGraw Hill, New York, 1980.
[21] Z. Alloui, T.H. Nguyen, E. Bilgen, Bioconvection of gravitactic micro-organisms in vertical cylinder, Int. Commun. Heat Mass Trans. 32 (2005) 739–747.
[22] A. Pellew, R.V. Southwell, On maintaining convective motion in a fluid heated from below, Proc. Roy. Soc. Series A, Math. Phys. Sci. 176 (1940) 312–343.
[23] T. Kawakubo, Y. Tsuchiya, Diffusion coefficient of paramecium as a function of temperature, J. Protozool. 28 (3) (1981) 342–344.
[24] Y. Mogami, A. Yamane, A. Gino, S.A. Baba, Bioconvective pattern formation of Tetrahymena under altered gravity, J. Exp. Biol. 207 (2004) 3349.